

# Prospects for the Detection of the Deep Solar Meridional Circulation

D. C. Braun, A. C. Birch

*NorthWest Research Associates, CoRA Division, 3380 Mitchell Lane, Boulder, CO 80301,  
USA*

dbraun@cora.nwra.com aaronb@cora.nwra.com

## ABSTRACT

We perform helioseismic holography to assess the noise in p-mode travel-time shifts which would form the basis of inferences of large-scale flows throughout the solar convection zone. We also derive the expected travel times from a parameterized return (equatorward) flow component of the meridional circulation at the base of the convection zone from forward models under the assumption of the ray and Born approximations. From estimates of the signal-to-noise ratio for measurements focused near the base of the convection zone, we conclude that the helioseismic detection of the deep meridional flow including the return component may not be possible using data spanning an interval less than a solar cycle.

*Subject headings:* Sun: helioseismology, interior

## 1. Introduction

Among all known large-scale flows in the Sun, the meridional circulation has particular significance because of its role in the transport of angular momentum and magnetic flux across a wide range of latitudes within the convection zone. Consequently, it is a significant component of models of the dynamics of rotating stellar convection zones, dynamos, and the solar cycle (Glatzmaier & Gilman 1982; Choudhuri et al. 1995; Dikpati & Gilman 2001; Wang et al. 1991, 2002; Hathaway et al. 2003, 2004; Dikpati & Gilman 2006, 2007).

Measurements of the surface manifestation of meridional circulation have typically indicated poleward flows between 10 and 20 m s<sup>-1</sup> (e.g. Hathaway 1996). Although frequencies of global p modes are insensitive (to first order) to the meridional circulation, the flows have been detected with a variety of local seismic methods (e.g. Giles et al. 1997,

1998; Braun & Fan 1998; González Hernández et al. 1999; Giles 2000; Haber et al. 2002; Hughes & Thompson 2003; Zhao & Kosovichev 2004; Chou & Ladenkov 2005; González Hernández et al. 2006; Švanda et al. 2007; Mitra-Kraev & Thompson 2007; González Hernández et al. 2008). Many of these studies have focused their attention on the meridional circulation near the surface (e.g. within a few tens of Mm below the surface), and only a few attempts have been made to deduce the properties of the deeper components. Among the most comprehensive analyses is the work of Giles (2000) which is based on models of time-distance measurements using over two years of Michelson Doppler Imager (MDI; Scherrer et al. 1995) Dopplergrams. These models included two general solutions for the meridional circulation as a function of depth and latitude: the first (hereafter “Giles’ model A”) without any constraint on mass conservations, and the second (Giles’ model B) with an imposed mass conservation. Only Giles’ model B exhibited a return flow while the other showed exclusively poleward flows throughout the convection zone. Each model was consistent with the travel-time measurements within their range of errors (Giles 2000).

In the frequency–wavenumber range of p modes propagating through the bottom half of the convection zone, the random noise present in most current helioseismic measurements is dominated by realization noise caused by stochastic excitation of the p modes near the solar surface. For the exploration of large-scale flows such as meridional circulation this can be reduced by observing more of the Sun (e.g. the far side of the Sun which is not currently accessible to helioseismic instruments) or by employing datasets with longer temporal duration. With over a decade of helioseismic observations from both the Global Oscillations Network Group (GONG; <http://gong.nso.edu/data>) and MDI (<http://soi.stanford.edu/data>) now available it is worthwhile to revisit the issue of the deep meridional circulation. In this paper, we explore the prospects for helioseismic detection of the return component of the meridional circulation in the deep solar convection zone by applying helioseismic holography to MDI observations to assess the random noise in travel-time shifts which would form the basis for the inference of large-scale flows. Our analysis and resulting noise estimates are described in § 2. We estimate the expected signal from a plausible return component of meridional circulation using forward modeling procedures described in § 3. This is followed in § 4 by a discussion of the implications of these results.

## 2. Noise Assessment

Helioseismic holography (hereafter HH) is a method which computationally extrapolates the surface acoustic field into the solar interior (Lindsey & Braun 1997, 2000) in order to estimate the amplitudes of the waves propagating into and out of a focus point at a chosen

depth and position in the solar interior. The magnitudes and phases of these amplitudes, called the ingressions and egressions, are used to detect flows and other perturbations to the waves. The method employed for horizontal flow diagnostics is based on the egressions and ingressions computed in the *lateral vantage* employing pupils spanning 4 quadrants extending in the east, west, north and south directions from the focus (Braun et al. 2004; Lindsey & Braun 2004; Braun et al. 2007). In the lateral vantage, the p modes sampled by the pupil propagate through the focal point in directions inclined up to  $\pm 45^\circ$  from the direction parallel to the surface (see Figure 3 of Braun et al. 2007). A difference in the travel times between waves traveling from one pupil to its opposite and waves traveling in the reverse direction is produced by flows along the path of the waves. In particular, the travel time differences,  $\delta\tau_{\text{ew}}$  and  $\delta\tau_{\text{ns}}$  derived from the east–west and north–south quadrant pairs, respectively, provide the HH signatures sensitive to the two components of the horizontal flow. The sign of the travel-time difference is such that a northward velocity component will produce a negative value of  $\delta\tau_{\text{ns}}$ . The lateral-vantage geometry samples more than 70% of the wave modes which pass through the focus. The remaining waves, propagating more vertically than the waves appearing in the pupil, are substantially less sensitive to horizontal flows near the focus. Table 1 lists the focus depths and the pupil radii used in this study. The pupil radii are defined from ray theory. The range of (spherical-harmonic) mode degrees ( $\ell$ ) at 4 mHz, selected by each pupil, is also listed in the table. The lower  $\ell$  value denotes the modes propagating at  $\pm 45^\circ$  from the horizontal direction which propagate through the focus and reach the surface at either the inner or outer pupil radius. The highest  $\ell$  value listed indicates modes propagating horizontally through the focus. The focus depths extend down to the base of the convection zone. However, the analysis is conceptually similar to previous near-surface measurements (Braun et al. 2007).

Three weeks of full disk Dopplergrams with one minute cadence, obtained from MDI were used in this study. The data set spans the interval from 1996 June 25 to July 16, and coincides with a period of very low magnetic activity on the Sun. Smaller spans of data at other epochs (2002 March and 2003 October) were also examined. Travel-time maps made at all three epochs exhibit similar noise characteristics, and we show here only the results using the 1996 data. The following steps summarize the general data reduction: 1) a projection of each 24 hr segment of full-disk data onto nine Postel projections (each extending  $180^\circ \times 180^\circ$ ) centered on grid points separated by  $40^\circ$  in heliographic latitude and central meridian distance referenced to midday and rotating with the Carrington rate, 2) temporal detrending by subtraction of a linear fit to each pixel signal in time, 3) removal of poor quality images, identified by a five- $\sigma$  deviation of any pixel from the linear trend, 4) Fourier transform of the data in time, 5) extraction of the frequency bandpass spanning 2.5 to 5.5 mHz, 6) computation of Green’s functions over the appropriate pupil, 7) com-

putation of ingress and egress amplitudes by a 2D convolution of the data with the Green’s functions, 8) computation of the travel-time difference maps, and 9) extraction and remapping of the central  $40^\circ \times 40^\circ$  portion of each region to form mosaics in heliographic coordinates spanning  $120^\circ \times 120^\circ$ . The Green’s functions (step 6) were computed using the eikonal approximation (Lindsey & Braun 1997, 2000) in spherical coordinates. The large size of the Postel’s projections is dictated by the large pupil required for the deepest foci in Table 1. The 2D convolution (step 7) is a time-saving convenience, appropriate for the type of preliminary noise estimates we are interested in, but distorts the resulting travel-time difference maps. This occurs because of a geometrical mismatch between the fixed annular pupil assumed for the convolution operation and the correct pupil whose shape varies with position in the Postel projection. This deviation worsens as the horizontal position of the focus is moved away from the central (tangent) point of the Postel projection, and the effects of this can therefore be constrained by combining maps made using multiple locations of the tangent point. The consequences of this distortion for the results presented here are discussed below.

Figure 1 shows selected maps of the mean  $\delta\tau_{\text{ns}}$  and standard deviation  $\sigma_0$  of the north-south travel-time difference over twenty consecutive (24-hr duration) sets of measurements. Each map covers an area of  $120^\circ$  in central meridian distance (CMD) and heliographic latitude (B). The maps for one day of data (June 27) were not included in further analysis due to an anomalously high amount of poor images. Near the surface (e.g. Figure 1a), the meridional flow produces a distinct negative (positive) travel-time difference in the north (south) hemisphere. As the focus depth increases, this signature becomes less visible. A distinct pattern near the poles is also evident and increases significantly with greater focus depth. This pattern is opposite in sign of the meridional signature and is clearly an artifact centered on the position of disk center (about  $+3^\circ$ ) as observed by MDI.

Remarkably, the maps of the standard deviation (Figs 1d - 1f) indicate that, apart from the vicinity of the solar limb, the noise for a single travel-time measurement is fairly constant ( $\sigma_0 \approx 4\text{sec}$ ) with focus depth. There is a granularity in these maps which becomes coarser with depth and is related to the increase in the horizontal wavelength of the modes used to make the measurements. An increase in the standard deviation near the solar limb is evident. In addition, there is a noticeable excess of  $\sigma_0$  near positions (CMD, B) =  $(\pm 20^\circ, \pm 20^\circ)$  which are the corners of the individual subregions of the mosaic. The noise in these corners is about 15% above the values near the Postel tangent points for all focus depths used here. This feature likely results from the use of the 2D convolution of Postel’s projections described earlier.

Due to signal-to-noise issues we assume any current or future attempt to deduce proper-

ties of the deep meridional circulation will make use of longitudinal averaging and very likely also involve at least modest smoothing in latitude. Figure 2 shows the standard deviation ( $\sigma_a$ ) of averages of  $\delta\tau_{\text{ns}}$  over strips spanning  $120^\circ$  in CMD and  $15^\circ$  in B. Unlike the standard deviation ( $\sigma_0$ ) corresponding to specific horizontal focus positions which show little or no variation with focus depth, the standard deviation of the mean ( $\sigma_a$ ) increases with depth at all latitudes. This is a consequence of having fewer independent measurements within a fixed area as the depth increases and is analogous to the common problem in global helioseismology of having fewer modes in which to deduce either structural perturbations or flows at greater depths within the Sun. There is also an increase in noise for measurements at high latitudes, consistent with the maps of  $\sigma_0$  (Figure 1). Significantly, the values of  $\sigma_a$  for the  $15 - 30^\circ$  strips are very close to the results for the  $0 - 15^\circ$  strip. This offers some assurance that the contribution of noise due to the 2D convolution (which should preferentially influence the  $15 - 30^\circ$  strip) does not add substantially to the results shown in Figure 2.

### 3. Forward Models

We use both the Born and ray approximations to estimate the travel-time shifts that would be caused by a return flow near the base of the convection zone. For a discussion of the ray approximation see Giles (2000). We used the numerical approach of Christensen-Dalsgaard et al. (1989) for computing ray paths in spherical geometry.

For this letter we also make rough estimates of the sensitivity of HH travel times to weak, steady, and horizontally uniform flows by approximating the convection zone as a plane-parallel layer. The functions which describe the linear sensitivity of the power spectrum to a horizontally uniform flow can be computed using a generalization of the Born-approximation based approach of Gizon & Birch (2002) and Birch & Gizon (2007). We used the normal-mode summation Green’s functions from Birch et al. (2004), though with the eigenfunctions for a spherical Sun in place of those for a plane-parallel version of model S. We used the source model of Birch et al. (2004). Changes in the the power spectrum may easily be related to changes in the ingress-ion-egression correlation through the expression for the expectation value of the correlation. The result is a set of sensitivity kernels which relate the correlations (and thus the travel-time shifts) with the flows.

Using the sensitivity functions we estimate the travel-time shifts caused by deep return flows of the form  $v(z) = A \cos\{\pi(r - r_c)/\Delta r\}$  for  $r_c < r < r_c + \Delta r$  and  $v(z) = 0$  otherwise. Here  $r_c = 496$  Mm is the radius of the base of the convection zone,  $\Delta r$  is the thickness of the return flow, and  $A$  is the maximum amplitude of the flow (Giles’ model B can be roughly approximated with  $A \approx 3$  m s $^{-1}$  and  $\Delta r \approx 60$  Mm). Figure 3 shows travel-time

differences, for two focus depths, as a function of  $\Delta r$ , predicted from the two methods. It is noteworthy that the times computed under the Born approximation can differ substantially from those than predicted by the ray approximation. Much of the sensitivity in the Born approximation lies below the lower turning point of the corresponding ray. In addition, for a sufficiently thick return flow the Born travel-time shifts are greater for the shallower focus depth than for the deeper focus depth. The deeper measurements use waves of higher phase speed, which undergo a smaller phase shift in a horizontally uniform flow.

#### 4. Discussion

To estimate the amount of data needed for a detection of the return flow, we conservatively assume that a successful detection requires a signal-to-noise ratio (SNR) of three for travel-time measurements near the base of the convection zone. Thus for the types of return flows shown in Figure 2, we require a measurement precision on the order of .01 seconds. Given a random noise of 0.6 seconds for a single day for a HH measurement over a  $15^\circ$  strip (Figure 2), it is apparent that at least 12 years of uninterrupted data is needed for a detection of a mean return flow with characteristics similar to Giles’ model B using the results of the ray approximation (i.e. a travel-time shift of 0.027 seconds), while the more confined flows to the left of the vertical line would require on the order of hundreds of years. These estimates are derived assuming the error in the mean flows decreases with the square root of the length of the time series (Gizon & Birch 2004). Combining data from both hemispheres and sacrificing some latitudinal resolution (e.g. to  $30^\circ$ ) it should be possible to (roughly) halve the required duration. We therefore tentatively conclude that a  $3\sigma$  detection of a return flow of a magnitude similar or smaller than Giles’ model B is possible only with an amount of data comparable or greater than a solar cycle.

The additional noise contributions or systematic errors due to analysis artifacts or details of the modeling procedures are not considered here, so that the results represent a “best-case” scenario. We anticipate that high-quality measurements spanning a range of depths will actually be needed to construct a model of the flow. Our emphasis on the SNR of the individual measurements is based on the relative “completeness” of lateral-vantage HH in that a single ingress–egression correlation efficiently samples and combines most of the waves propagating through a particular depth. We therefore assume that the uncertainty in the inferred flow at the base of the convection zone will be dominated by the random noise contribution to measurements focused at that position.

It is worthwhile to compare our results with uncertainties in other helioseismic measurements of flows near the base of the convection zone. From inversions of global-mode

frequency splittings, Howe et al. (2000) derive  $1\sigma$  errors of inverted rotation rates at a depth of 195 Mm of about 1 nHz (corresponding to  $4.4 \text{ m s}^{-1}$ ) for 72-day sets of MDI observations with an averaging kernel approximately 50 Mm wide (FWHM) in depth and about  $15^\circ$  wide in latitude. A  $3\sigma$  detection of an average  $1.5 \text{ m s}^{-1}$  zonal flow over this range in depth and latitude would therefore require about 15 years of frequency-splitting measurements which agrees very well with the estimate presented here.

Although direct measurements of temporal variability of the return component over timescales equal to or less than a solar cycle appear unlikely, we note that some inferences about variability could be made using shallower flow measurements and assuming mass conservation, as did Giles (2000). Regardless of possible temporal variability, it is likely well worth the effort to carry out analyses and modeling of existing decade-length helioseismic observations to either detect or constrain the mean return component. However, we note that there are a considerable number of potential qualifications to the rather simple estimates derived here. Some of these involve issues of the resolution of the models (e.g. the ability to infer the existence of multiple meridional cells or sharp gradients of flow in latitude or depth). In addition, we expect considerable challenges to the probing of any flows in the deep convection zone raised by the need to understand and remove possible artifacts and systematic effects. Some of these effects are visible as systematic differences between inferred flows using separate but contemporary datasets (González Hernández et al. 2006). These differences are often of the order of a few  $\text{m s}^{-1}$  which, while troublesome for probing even the near-surface layers, are clearly disastrous for the unambiguous identification of a return flow of comparable or smaller magnitude. The critical need for multiple sources of long-duration helioseismic observations combined with careful artifact identification and correction procedures in reducing both systematic effects and random noise should be clear.

We appreciate useful discussions with M. Woodard. DCB and ACB are supported by funding through NASA contract NNH05CC76C and NSF grant AST-0406225, and a subcontract through the NASA sponsored HMI project at Stanford University awarded to NWRA.

## REFERENCES

- Birch, A. C. & Gizon, L. 2007, *Astron. Nachr.*, 328, 228
- Birch, A. C., Kosovichev, A. G., Duvall, T. L., Jr. 2004, *ApJ*, 608, 580

- Braun, D. C., Birch, A. C., & Lindsey, C. 2004, ESA SP-559: SOHO 14 Helio- and Astero-  
seismology: Towards a Golden Future, 14, 337
- Braun, D. C., Birch, A. C., Benson, D., Stein, R. F., & Nordlund, Å. 2007, ApJ, 669, 1395
- Braun, D. C., & Fan, Y. 1998, ApJ, 508, L105
- Braun, D. C., & Lindsey, C. 2003, ESA SP-517: GONG+ 2002. Local and Global Helioseis-  
mology: the Present and Future, 12, 15
- Chou, D.-Y., & Ladenkov, O. 2005, ApJ, 630, 1206
- Choudhuri, A. R., Schussler, M., & Dikpati, M. 1995, A&A, 303, L29
- Christensen-Dalsgaard, J., Thompson, M. J., Gough, D. O. 1989, MNRAS, 238, 481
- Christensen-Dalsgaard, J., et al. 1996, Science, 272, 1286
- Dikpati, M., & Gilman, P. A. 2001, ApJ, 559, 428
- Dikpati, M., & Gilman, P. A. 2006, ApJ, 649, 498
- Dikpati, M., & Gilman, P. A. 2007, Sol. Phys., 241, 1
- Giles, P. M. 2000, Ph.D. Thesis, Stanford University
- Giles, P. M., Duvall, T. L., Jr., & Scherrer, P. H. 1998, Structure and Dynamics of the  
Interior of the Sun and Sun-like Stars, 418, 775
- Giles, P. M. Duvall, T. L., Jr., Scherrer, P. H., & Bogart, R. S. 1997, Nature, 390, 52
- Gizon, L. & Birch, A.C. 2002, ApJ, 571, 966
- Gizon, L., & Birch, A. C. 2004, ApJ, 614, 472
- Glatzmaier, G. A., & Gilman, P. A. 1982, ApJ, 256, 316
- González Hernández, I., Kholikov, S., Hill, F., Howe, R., & Komm, R. 2008, ArXiv e-prints,  
808, arXiv:0808.3606
- González Hernández, I., Komm, R., Hill, F., Howe, R., Corbard, T., & Haber, D. A. 2006,  
ApJ, 638, 576
- González Hernández, I., Patrón, J., Bogart, R. S., & The SOI Ring Diagram Team 1999,  
ApJ, 510, L153



- Haber, D. A., Hindman, B. W., Toomre, J., Bogart, R. S., Larsen, R. M., & Hill, F. 2002, *ApJ*, 570, 855
- Hathaway, D. H. 1996, *ApJ*, 460, 1027
- Hathaway, D. H., Nandy, D., Wilson, R. M., & Reichmann, E. J. 2003, *ApJ*, 589, 665
- Hathaway, D. H., Nandy, D., Wilson, R. M., & Reichmann, E. J. 2004, *ApJ*, 602, 543
- Howe, R., Christensen-Dalsgaard, J., Hill, F., Komm, R. W., Larsen, R. M., Schou, J., Thompson, M. J., & Toomre, J. 2000, *Science*, 287, 2456
- Hughes, S. J., & Thompson, M. J. 2003, *GONG+ 2002. Local and Global Helioseismology: the Present and Future*, 517, 307
- Lindsey, C. & Braun, D. C. 1997, *ApJ*, 485, 895
- Lindsey, C. & Braun, D. C. 2000, *Sol. Phys.*, 192, 261
- Lindsey, C. & Braun, D. C. 2004, *ApJS*, 155, 209
- Mitra-Kraev, U., & Thompson, M. J. 2007, *Astronomische Nachrichten*, 328, 1009
- Scherrer, P. H. et al. 1995, *Sol. Phys.*, 162, 129
- Švanda, M., Zhao, J., & Kosovichev, A. G. 2007, *Sol. Phys.*, 241, 27
- Wang, Y.-M., Lean, J., & Sheeley, N. R., Jr. 2002, *ApJ*, 577, L53
- Wang, Y.-M., Sheeley, N. R., Jr., & Nash, A. G. 1991, *ApJ*, 383, 431
- Zhao, J., & Kosovichev, A. G. 2004, *ApJ*, 603, 776

Table 1. Pupil size and mode degrees

Depth (Mm)	Pupil radii (degrees)	$\ell$ @ 4mHz
30	1.3 - 10.5	166 - 235
37	1.7 - 12.9	145 - 205
45	2.0 - 15.4	128 - 180
54	2.4 - 18.2	113 - 159
64	2.9 - 21.1	100 - 142
76	3.4 - 24.1	89 - 127
88	4.0 - 26.5	81 - 114
100	4.5 - 29.2	73 - 104
114	5.2 - 32.0	66 - 93
130	5.9 - 35.2	59 - 84
150	6.8 - 41.4	52 - 74
170	7.7 - 48.1	46 - 66
190	8.6 - 54.9	41 - 58
200	9.1 - 57.1	39 - 55

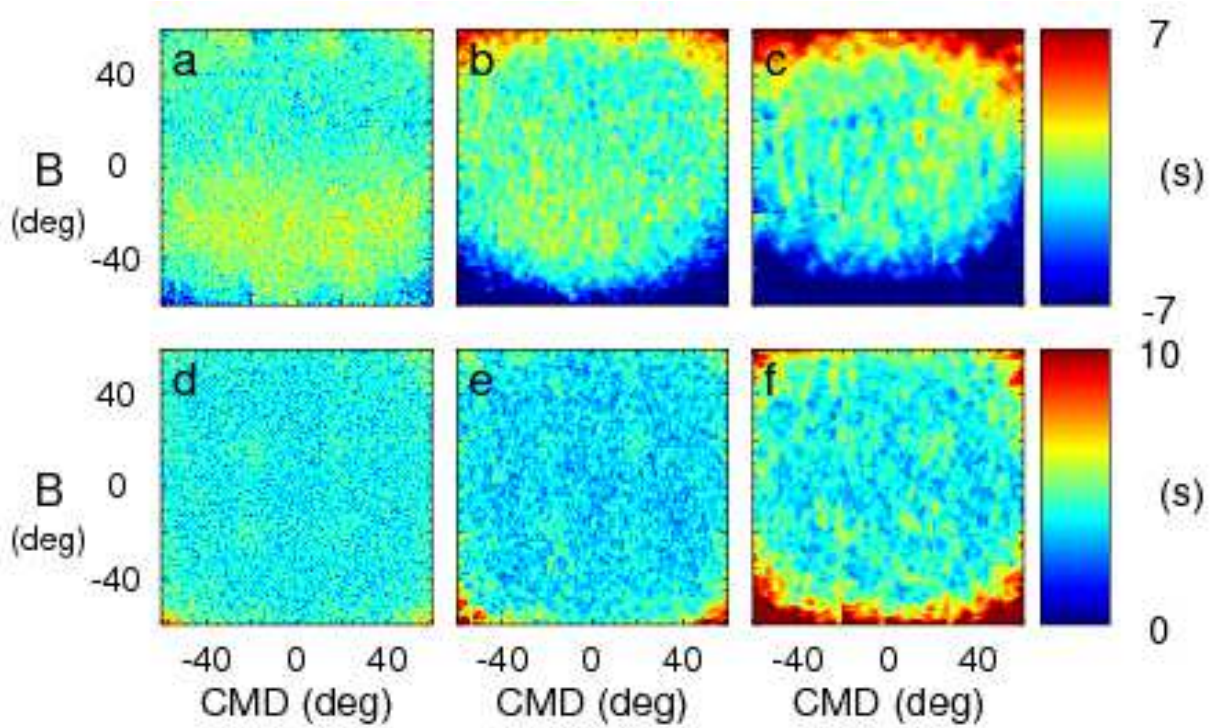


Fig. 1.— Maps of the mean (panels a-c) and standard deviation (panels d-f) of north-south travel-time differences for twenty consecutive 24-hr measurements. From left to right the focus depths of the measurements are 30, 100, and 200 Mm respectively.

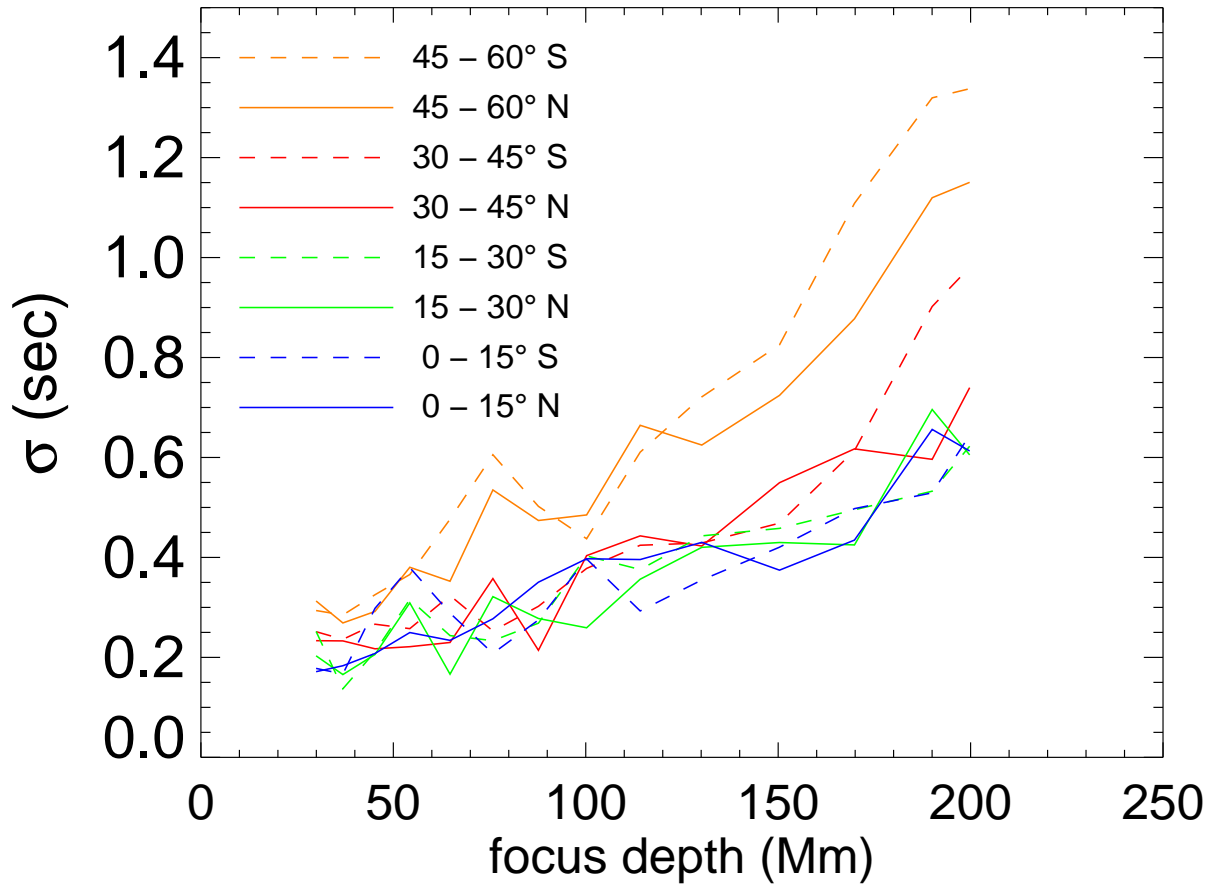


Fig. 2.— The standard deviation (over twenty consecutive 24-hr measurements) of the mean north-south travel-time difference averaged over a strip of the Sun spanning 15 degrees in latitude and 120 degrees in central meridian distance. Different colors indicate different latitudes of the center of the strip, while solid (dashed) lines indicate the southern (northern) hemisphere. In general, the mean-standard-deviation increases with the depth of the focus, and also increases at high latitudes.

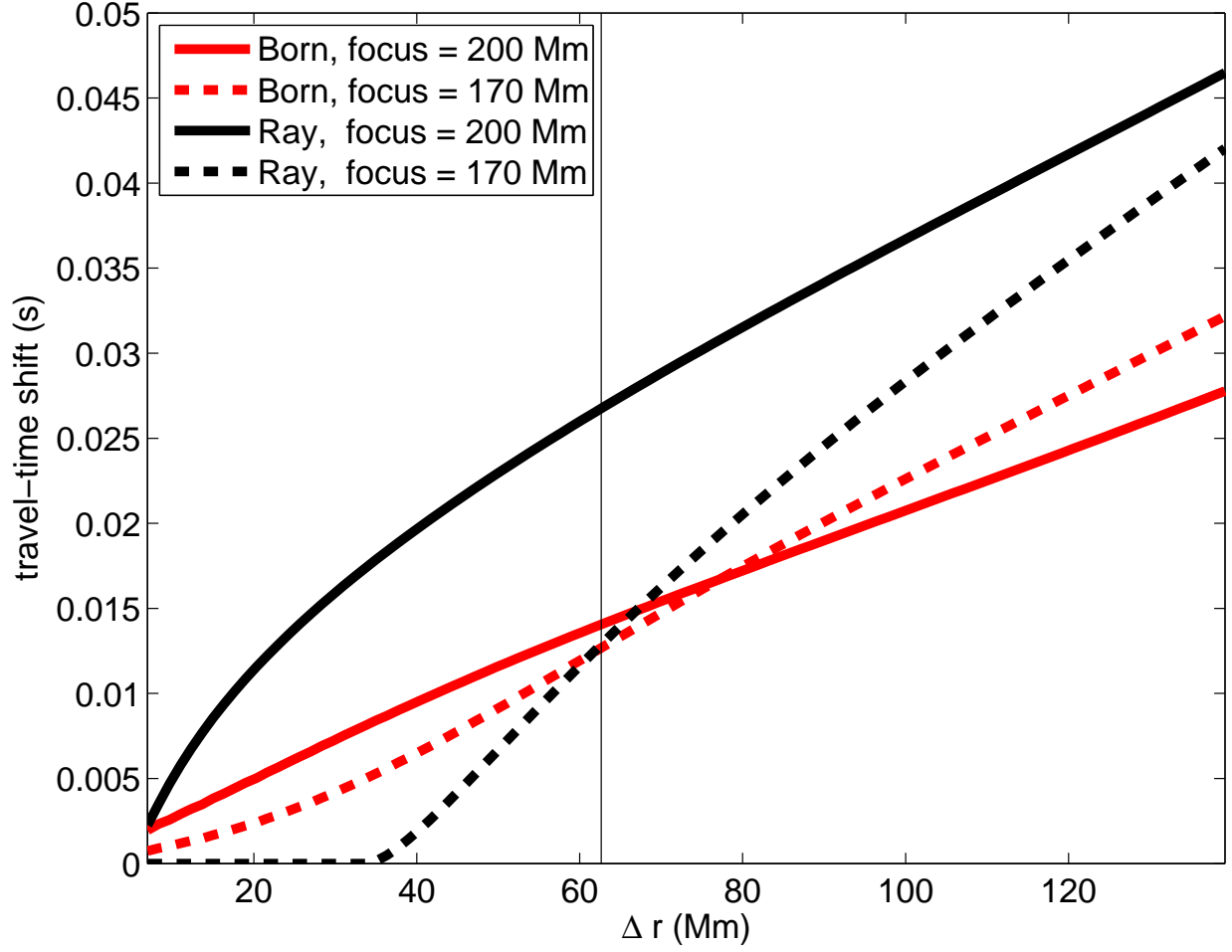


Fig. 3.— Expected north–south travel-time difference as functions of the width of a hypothesized meridional return flow at the base of the convection zone with a peak value of  $3 \text{ m s}^{-1}$  (see text). The flow is set to zero in the radiative zone. The red (black) lines show the results of a Born (ray) approximation calculation, and the the solid (dashed) lines show the results for focus depths of 200 (170) Mm below the surface. The vertical line indicates the width which roughly corresponds to Giles’ model B.